CrossMark

Evaluation of climatological tropical cyclone activity over the western North Pacific in the CORDEX-East Asia multi-RCM simulations

Chun-Sil Jin[1,2] · Dong-Hyun Cha[1] · Dong-Kyou Lee[2] · Myoung-Seok Suh[3] ·
Song-You Hong[4] · Hyun-Suk Kang[5] · Chang-Hoi Ho[2]

Abstract The ability of five regional climate models (RCMs), within the Coordinated Regional Climate Downscaling Experiment (CORDEX) for East Asia, to simulate tropical cyclone (TC) activity over the western North Pacific is evaluated. All RCMs are performed at ~50 km resolution over the CORDEX-East Asia domain, and are driven by the ECMWF Interim Re-Analysis (ERA-Interim) for the period 1989–2008. ERA-Interim sea surface temperature is prescribed as the lower boundary. Performances of the individual RCMs and multi-RCM ensemble mean are investigated in detail for 20-year climatology, intensity, and interannual variability of TC activity compared to observational datasets. Although most of the individual RCMs show significant biases and underestimate TC intensity due to horizontal resolutions still too low to resolve the most intense observed TCs, they reasonably capture the observed climatological spatial distribution and interannual variability of TC activity. The multi-RCM ensemble mean based on the model performance generally outperforms most of the individual models with smaller biases and higher correlation on the spatial and temporal variation of TC activity. This ensemble mean reduces the uncertainty in the simulated TC activity by a single RCM. These analyses suggest that the multi-RCM ensemble within CORDEX-East Asia can be applied to provide more reliable and credible estimation of future TC activity over the western North Pacific due to climate change.

Keywords CORDEX · Regional climate modeling · Model evaluation · Tropical cyclone · Western North Pacific

1 Introduction

Many previous studies have examined the impact of global warming on tropical cyclone (TC) activity using climate models. Low-resolution general circulation models (GCMs) have been shown to be capable of producing TC-like vortices and providing the large-scale variables associated with TC activity (Bengtsson et al. 1982; Camargo 2013; Vitart et al. 1997). They have effectively provided future climate change projections, but their coarse resolutions prevent them from resolving aspects of individual TC structures (LaRow et al. 2008). Recognizing this limitation, high-resolution GCMs have been utilized to provide more realistic TC characteristics in many institutes (Manganello et al. 2012; Murakami et al. 2012a, b; Oouchi et al. 2006; Strachan et al. 2013; Walsh et al. 2014; Wehner et al. 2014; Zhao and Held 2012; Zhao et al. 2009). However, these experiments are still burdensome due to large computational resources required to run the high-resolution GCMs for multi-decadal simulations.

An alternative is to embed high-resolution regional models within GCMs producing more highly resolved TCs. This approach includes dynamical and statistical-dynamical downscaling techniques. The dynamical downscaling

✉ Dong-Hyun Cha
dhcha@unist.ac.kr

1   School of Urban and Environmental Engineering, Ulsan National Institute of Science and Technology, 50 UNIST-gil, Eonyang-eup, Ulju-gun, Ulsan 689-798, Republic of Korea

2   School of Earth and Environmental Sciences, Seoul National University, Seoul, Republic of Korea

3   Department of Atmospheric Science, Kongju National University, Kongju, Republic of Korea

4   Korea Institute of Atmospheric Prediction Systems, Seoul, Republic of Korea

5   National Institute of Meteorological Research, Jeju, Republic of Korea

technique can provide more detailed information on TC activity over a region of interest in the GCM output using the high-resolution regional climate model (RCM) (Au-Yeung and Chan 2012; Bender et al. 2010; Camargo et al. 2007; Cha et al. 2011b; Feser and von Storch 2008; Knutson et al. 2007; Lee et al. 2013; Wu et al. 2014). This technique has been providing useful insights into the dependence of TC activity on climate. As a variant of dynamical downscaling, the statistical-dynamical downscaling technique described in Emanuel et al. (2008) can generate a very large number of synthetic TCs with more realistic intensity based on GCM environmental fields using simpler embedded models. It can also avoid the limitations on intensity simulations in the dynamical downscaling using the RCM. However, these two techniques present some drawbacks such as (1) an inconsistency in the physics between the GCMs and RCMs, (2) a lack of feedback from the RCMs to the GCMs, and (3) inherent uncertainties and systematic errors induced by single RCMs. In case of the dynamical downscaling, the first and second issues can be resolved by using a unified single model system across a range of spatial scales (convective scale to climate system) with an identical physics package for global and regional models [e.g., Model Prediction across Scales (MPAS, Skamarock et al. 2012) and Global/Regional Integrated Model system (GRIMs, Hong et al. 2013a)]. The third issue that makes it difficult to assess the significance and reliability of their future projections of TC activity, can be resolved by using multi-RCM ensemble.

In order to alleviate the uncertainties of the single RCM, the multi-RCM ensembles obtained by downscaling GCMs for future climate projections, have been generated through several international projects during the past decade (Christensen et al. 2007; Fu et al. 2005). Recently, the Coordinated Regional Climate Downscaling Experiment (CORDEX) was organized as an international coordinated framework to produce high-resolution regional climate change projections based on the Coupled Model Intercomparison Project Phase 5 (CMIP5) using multi-RCMs (Giorgi et al. 2009). CORDEX-East Asia, which is the East-Asian branch of the CORDEX initiative, is suitable to provide future projections of TC activity over the western North Pacific (WNP) because its domain covers a major part of this basin with reasonable fine-resolution in simulating TCs on the multi-decadal time scale. However, RCMs within CORDEX-East Asia have not been evaluated for their ability to simulate TC activity over the WNP. They have been only just evaluated for simulating the precipitation and temperature over East Asia (Huang et al. 2015; Lee and Hong 2014; Oh et al. 2013; Park et al. 2013; Suh et al. 2012; Zou et al. 2014). The model evaluation is a fundamental step prior to assessing climate change projections, since RCMs play critical roles in decision making

processes with climate information (Hong et al. 2010; Kim et al. 2014b; Suh et al. 2012). Thus, it is necessary to objectively evaluate the capability of RCMs in simulating WNP TC activity.

This study aims to evaluate the capability of five RCMs within CORDEX-East Asia and their ensemble mean to simulate WNP TC activity at spatial and temporal scales as compared to observation. Namely, we confirm whether CORDEX multi-RCM ensemble can be applied to provide more reliable and credible estimation of future TC activity over the WNP. This paper is organized as follows. In Sect. 2, the data, model, and methodology including detection of TCs is described. In Sect. 3, the climatology of the simulated TC activity and large-scale environment in the RCMs is presented and discussed. The intensity distribution and interannual variability of the simulated TCs are described. The summary and conclusion are given in Sect. 4.

2 Data and methodology

The best track data for WNP TCs was obtained from the Regional Specialized Meteorological Centers (RSMC) Tokyo—Typhoon Center for the period 1989–2008. This dataset contains 6-h latitude and longitude locations, minimum central pressure, maximum wind speed, etc. The location where an individual TC first attains tropical storm intensity (i.e., greater than 17 m s^{-1}) is set as the genesis point, so that the TCs include both tropical storms and typhoons. The analysis is focused on the TCs formed from June to November (JJASON) covering approximately 85 % of the total annual TCs over the WNP. To evaluate the performance of the models, simulated upper air fields are compared with the reanalysis driving forcings. In addition, the Climate Prediction Center Merged Analysis of Precipitation (CMAP) monthly data with 2.5° × 2.5° horizontal resolution (Xie and Arkin 1997) are used for precipitation evaluation.

In this study, five different RCMs [Hadley Centre Global Environmental Model version 3 regional climate model (HadGEM3-RA), Regional Climate Model (RegCM), Seoul National University Regional Climate Model (SNURCM), Weather Research and Forecasting model (WRF), and GRIMs] were used for the TC simulations. Details of their dynamics and physics are presented in Table 1. The RCM simulation covers the period 1989–2008, with lateral boundary forcing from the ERA-Interim reanalysis. A spectral nudging is implemented into all RCMs except HadGEM3-RA to reduce the systematic errors in long-term simulations. ERA-Interim SST data are prescribed as the model's lower boundary. RCMs were performed over the CORDEX-East Asia domain with ~50 km resolution. The almost identical setups (i.e., driving data,

Table 1 The main characteristics of the RCMs used in this study

	HadGEM3-RA	RegCM	SNURCM	WRF	GRIMs
Institute	National Institute of Meteorological Research	Kongju National University	Seoul National University	Seoul National University	Yonsei University
Dynamics framework	Non-hydrostatic	Hydrostatic	Non-hydrostatic	Non-hydrostatic	Hydrostatic
Projection resolution	Rotated pole 0.44° (~50 km)	Lambert conformal 50 km	Lambert conformal 50 km	Lambert conformal 50 km	Mercator 50 km
Vertical levels	38	18	24	27	22
Convection	Gregory and Rowntree (1990)	Emanuel (1991)	Kain (2004)	Kain (2004)	Hong and Pan (1998)
PBL	Lock et al. (2000)	Holtslag et al. (1990)	Hong et al. (2006)	Hong et al. (2006)	Hong et al. (2006)
Spectral nudging	No	Yes (full wind nudging)	Yes (full wind nudging)	Yes (full wind nudging)	Yes (rotational wind nudging only)
Reference	Davies et al. (2005)	Giorgi et al. (2012)	Lee et al. (2004)	Skamarock et al. (2008)	Hong et al. (2013b)
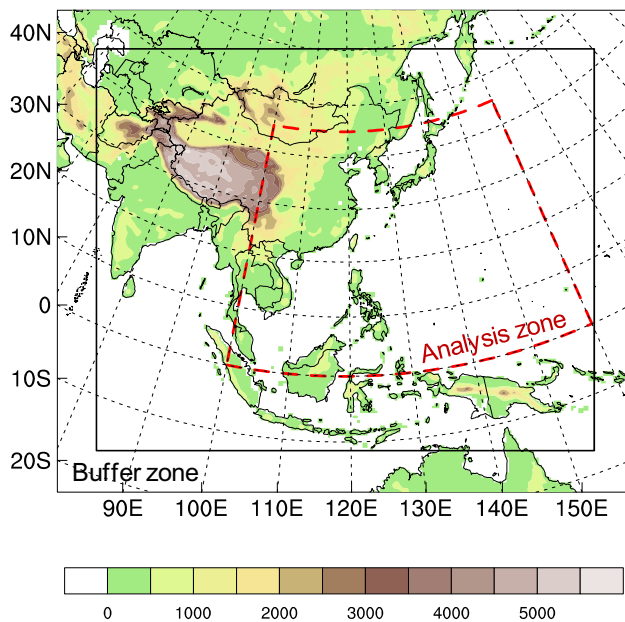
Fig. 1 The CORDEX-East Asia domain with topography (m) and western North Pacific area (*dashed line*)

simulation period, domain, and resolution) allows us to fairly assess the model performance and to reduce inherent uncertainty of single RCM in simulating TC by constructing multi-RCM ensemble. The model results have been interpolated onto the analysis domain (0–45°N, 100–160°E) of 0.5° to analyze WNP TC activity (Fig. 1). Since the analysis domain is smaller than the official WNP basin and the RCMs can be strongly influenced by the position of the boundary of the model domain, the observed and simulated TCs should be carefully analyzed (Camargo et al. 2007; Landman et al. 2005). To relieve this issue, the genesis and track position of observed TC advected from

the outside the analysis domain, are defined as the first and subsequent positions after crossing the boundaries of the analysis domain. Details of the RCM experiments are provided in Suh et al. (2012), except for HadGEM3-RA which is described in Davies et al. (2005).

The detection and tracking methods for simulated TCs used in this study are almost the same as that used in previous studies (Cha et al. 2011b; Jin et al. 2013): (1) the potential storm is a local minimum of sea level pressure; (2) the maximum surface wind exceeds the wind speed threshold; (3) the maximum relative vorticity at 850 hPa exceeds the vorticity threshold; (4) the sum of the temperature deviations at 200, 500, and 850 hPa exceeds the temperature anomaly threshold; (5) the maximum wind speed at 850 hPa is larger than that at 300 hPa; (6) the duration is not shorter than 2 d; (7) tracks are traced from these identified potential storms. Unlike the previous studies, the wind speed, vorticity, and temperature anomaly thresholds are defined as model-dependent thresholds proposed by Camargo and Zebiak (2002) to fairly compare the capability of the individual models to simulate TC activity. The vorticity threshold is defined as two standard deviation of 850-hPa relative vorticity over the WNP. The vertically integrated anomalous temperature is defined as one standard deviation of temperature at 200, 500, and 850 hPa over the WNP, due to the absence of variables at 300 and 700 hPa in the CORDEX-East Asia outputs. The wind speed threshold is defined as the sum of the oceanic global wind speed plus one standard deviation of the WNP wind speed. Here, the oceanic global wind speed value is estimated using the ratio of the global-mean wind speed to the wind speed averaged over the WNP (0–45°N, 100–160°E) in the ERA-Interim reanalysis data. However, since the estimated values in the models are much smaller than 17 m s^{-1}, which is the threshold given for a 50-km resolution model in

Table 2 Thresholds used for relative vorticity (10^{-5} s^{-1}), surface wind speed (m s^{-1}), and warm core (K) for defining TC in the WNP

	ERAI	HadGEM3-RA	RegCM	SNURCM	WRF	GRIMs
Vorticity	4.2	5.0	7.0	7.4	7.7	7.3
Temperature	0.9	0.5	0.5	0.6	0.5	0.6
Wind speed	10.3	**14.3**	**16.0**	**17.0**	**16.9**	**17.0**

Estimated values using ratio of WNP mean wind speed to global mean in the reanalysis are shown in bold

Walsh et al. (2007), we adjust the largest estimated value to 17 m s^{-1} and then modify the remaining estimated values using this ratio. The three threshold values for the five RCMs used in this study are given in Table 2.

To reduce the uncertainty of the single RCM, we construct the ensemble average of five RCMs using the performance-based ensemble averaging (PEA) method suggested by Suh et al. (2012). They showed that the PEA had the best skill among the various ensemble methods, regardless of variables and seasons. The PEA is calculated with different weighting using root-mean-square errors (RMSE) and spatial correlation coefficients between simulated and observed TC genesis densities in the analysis area, assuming that the simulation performance is inversely proportional to the RMSE but proportional to the correlation coefficient (Eqs. 1–3).

$$Pw_i = \frac{1.0}{(RMSE_i + 1.0)} Corr_i \tag{1}$$

$$NPw_i = \frac{Pw_i}{\sum_{i=1}^{N_M} Pw_i} \tag{2}$$

$$\tilde{M} = \sum_{i=1}^{N_M} NPw_i M_i \tag{3}$$

here, Pw_i, NPw_i, N_M, and M_i are weighting, normalized weighting, number of ensemble members, and variable for ith model, respectively. In order to analyze the performance of the PEA, we also calculate another ensemble average as a reference using equal-weighted averaging (EWA) method, which is commonly used in multi-model ensemble studies.

3 Results

3.1 Climatology of TC activity and their related large-scale environment

Figure 2 shows the 20-year mean TC genesis density from observations and the five RCMs. TC genesis density is displayed by binning the latitude and longitude positions into a 2.5° × 2.5° grid box; this method has been generally applied to the binning of TC data (Ho et al. 2013; Kim et al. 2010). In the observations, TC genesis locations are concentrated in a region between 5 and 25°N and three local maxima: the South China Sea (SCS; 115–120°E), the western part of the Philippine Sea (PS; 125–135°E), and Mariana Trench (around 145°E). HadGEM3-RA unrealistically underestimates the TC formations over most of the WNP compared to the observations. The mean seasonal total numbers are 18.1 and 4.6 in the observations and HadGEM3-RA, respectively (see Table 3). Two main TC genesis regions over the SCS and PS simulated by RegCM are slightly southward and eastward shifted compared to the observations, respectively. This pattern is consistent with what has been reported by previous studies using RegCM (Au-Yeung and Chan 2012; Huang and Chan 2014). Despite this systematic errors, RegCM reasonably reproduces observed pattern of TC genesis (spatial correlation is 0.85) and mean seasonal total numbers (18.9). SNURCM overestimates TC formation (22.0) over the entire WNP, but it captures well the observed main TC genesis areas over the PS and the SCS (spatial correlation is 0.89). The simulated TC genesis density by WRF agrees better with the observations than that by the other models in terms of both spatial distribution and genesis frequency. The spatial correlation of TC genesis density between WRF and the observations and mean total numbers are 0.89 and 17.6, respectively, which are the best statistics as compared to the other models. GRIMs has significant errors of simulating an unrealistic spatial pattern of TCs (spatial correlation is 0.49) and underestimating TC formations (14.6), especially over the PS. These results indicate that RegCM, SNURCM, and WRF are able to simulate TC formation over the WNP reasonably, while HadGEM3-RA and GRIMs have considerable systematic errors in the simulation of TC genesis.

For the EWA, the spatial correlation of TC genesis density with the observations increases to 0.91, since the negative biases over the SCS and the WNP in HadGEM3-RA and GRIMs are offset by the positive biases in SNURCM and RegCM. However, the EWA still underestimates the TC formations (15.9), especially over the PS due to the large systematic errors of HadGEM3-RA and GRIMs. In the PEA, the pattern and frequency of TC genesis over the WNP are considerably improved. The spatial correlation and mean total number are 0.92 and 17.4, respectively. The improved results by PEA are due to the higher weighting
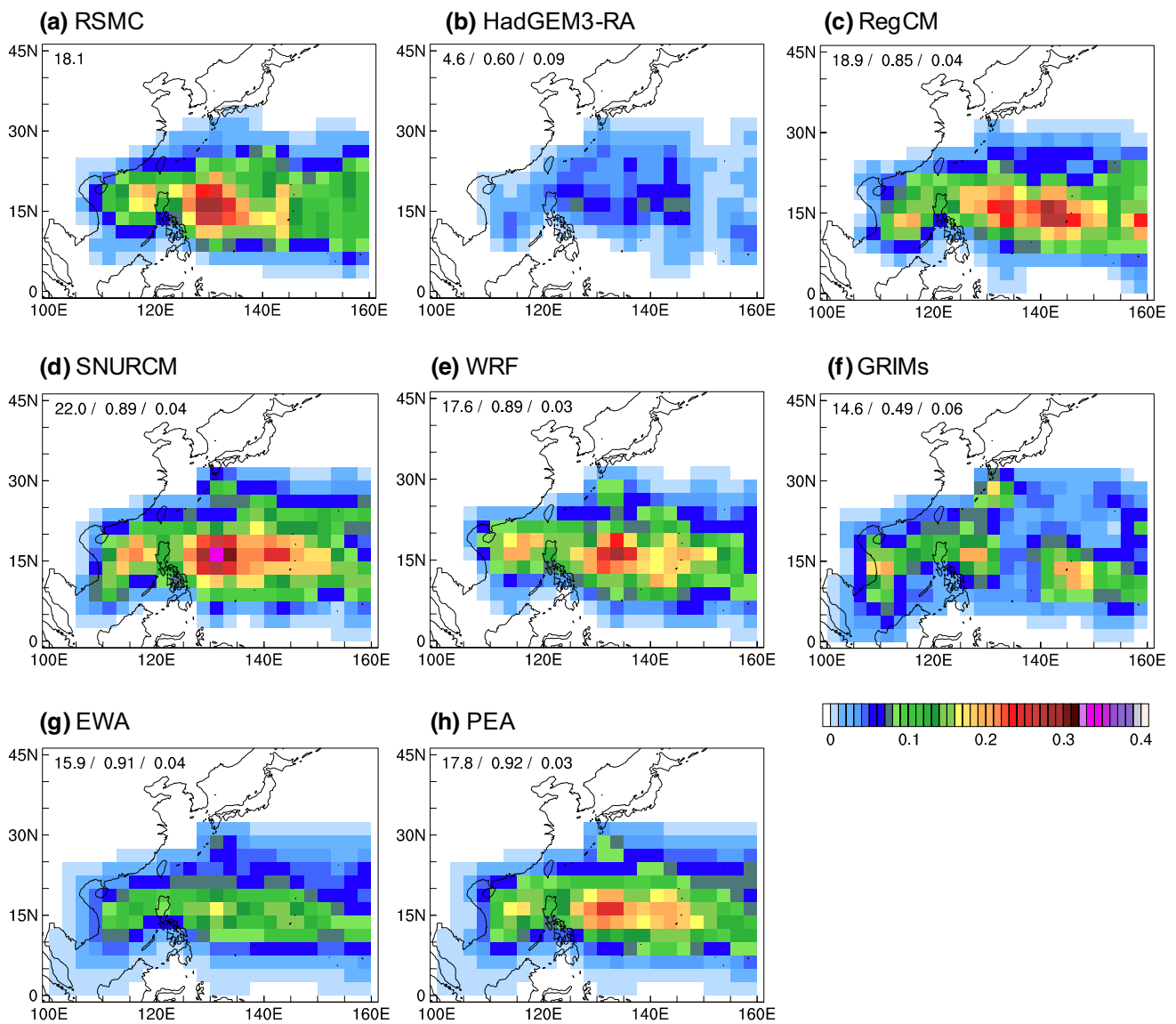
Fig. 2 Climatological mean of TC genesis density in **a** RSMC and **b–h** models for the period 1989–2008. Also listed in each panel are the values of mean genesis frequency, spatial correlation, and RMSE with RSMC

Table 3 Statistics for TC genesis and ACE during the period 1989–2008

	TC genesis					ACE				
	Mean	SD	RMSE	Tcorr	Slope	Mean	SD	RMSE	Tcorr	Slope
RSMC	18.1	4.3	–	–	−0.46	42.9	15.3	–	–	−1.04
HadGEM3-RA	4.6	2.9	14.0	0.38	0.00	2.3	1.6	43.0	0.61***	−0.05
RegCM	18.9	6.1	5.1	0.56**	−0.43	15.6	5.7	30.0	0.60***	−0.31
SNURCM	22.0	4.6	6.1	0.44*	−0.27	29.2	8.6	16.9	0.79***	−0.18
WRF	17.6	4.3	4.0	0.53**	−0.20	25.5	8.4	21.3	0.56**	0.25
GRIMs	14.6	4.3	7.9	0.07	0.14	16.1	8.8	31.3	0.40*	0.09
EWA	15.3	3.3	4.3	0.58***	−0.17	17.9	5.4	27.6	0.74***	−0.12
PEA	17.8	3.9	3.4	0.64***	−0.27	21.4	6.3	24.1	0.77***	−0.09

*,** and *** The value that the correlation is significant at the 90, 95, and 99 % level, respectively

SD and Tcorr indicate standard deviation and temporal correlation, respectively
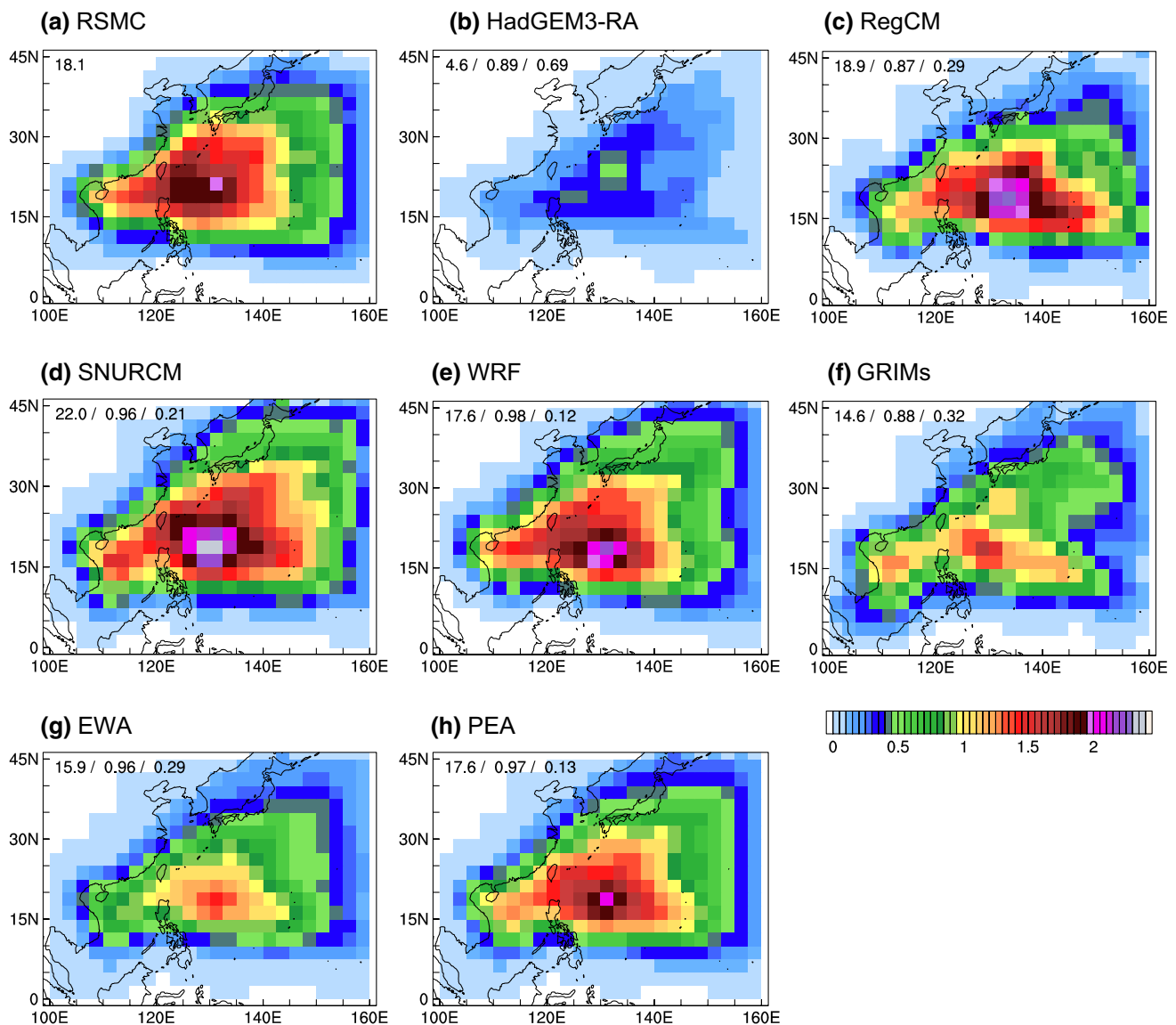
Fig. 3 As in Fig. 2, but for TC track density

coefficient for RegCM, SNURCM, and WRF, which have a better performance simulating the WNP TC genesis.

Similar to TC genesis, simulated track densities simulated by HadGEM3-RA and GRIMs have relatively large errors, while simulated those by the other three models are comparable to the observations (Fig. 3). TC track density is computed by binning 6-hourly TC positions onto the corresponding grid boxes. The same TC migrating in the same grid box is counted only once. HadGEM3-RA considerably underestimates track densities over the entire WNP because it cannot resolve the relevant TC formations there as shown in Fig. 2b. RegCM overestimates the track density over the eastern part of the WNP due to the exaggerated TC genesis there (Fig. 2c). In addition, RegCM slightly underestimates the track density over the East Asian coastal regions (20–35°N, 120–140°E), which is possibly associated with the low TC formation frequency over the PS. SNURCM reasonably simulates the spatial distribution of tracks, but generally overestimates TC tracks over the SCS and the entire WNP due to the formation of more simulated TCs therein as shown in Fig. 2d. WRF reproduces the track density most realistically compared to the other models. GRIMs tends to underestimate TC tracks near the East Asian coastal regions, which is related to the largely underestimated formations of TCs over the PS as shown in Fig. 2f. In the EWA, the ensemble mean track density is underestimated over most of the WNP because of the impacts of HadGEM3-RA and
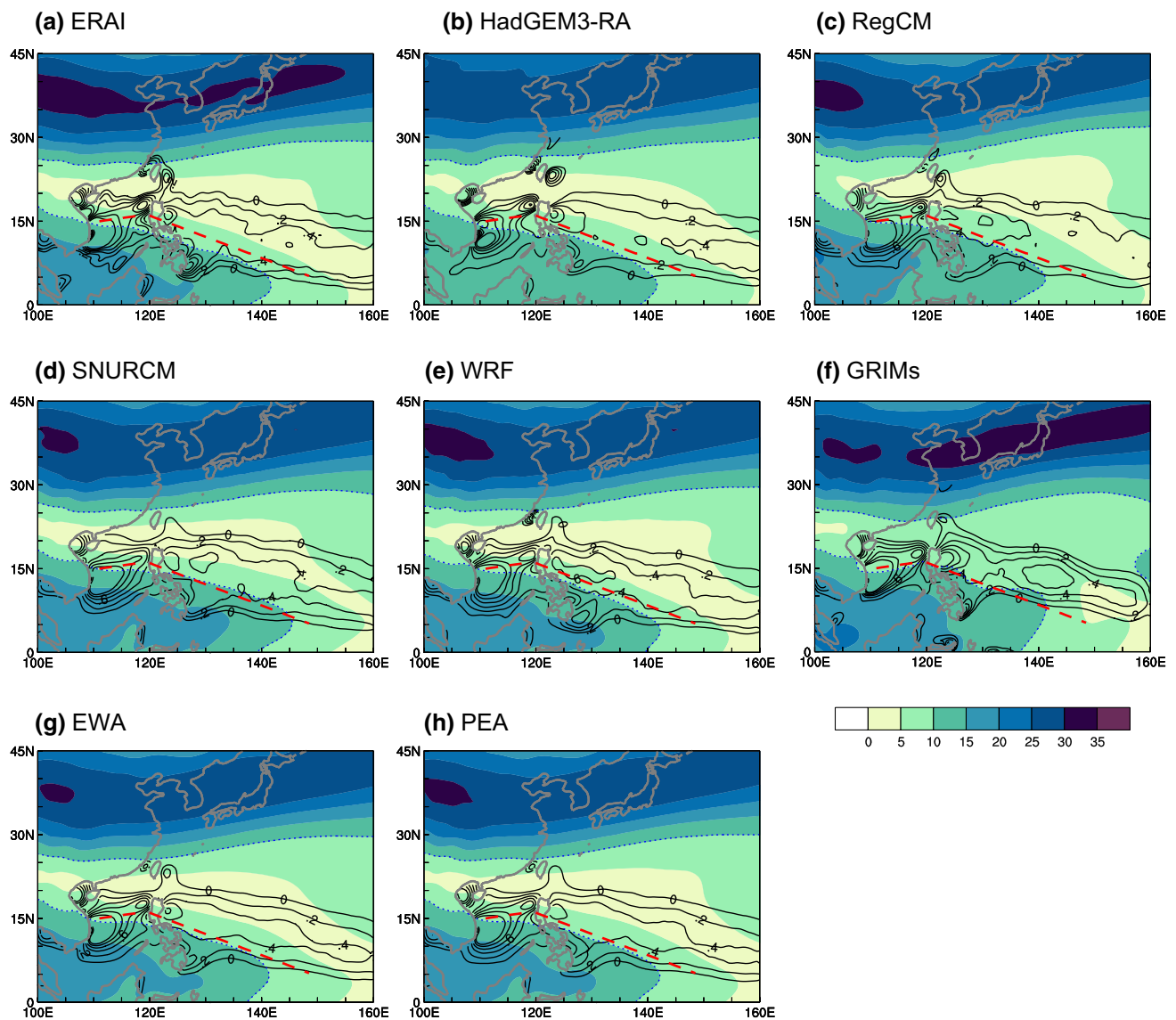
Fig. 4 Climatological mean of vertical wind shear (m s^{-1}; *shading*) and positive 850-hPa relative vorticity (10^{-5} s^{-1}; *contour*) in **a** ERA-Interim and **b–h** models for the period 1989–2008. *Red dashed lines* denote the axis of the monsoon trough in the reanalysis, which is determined with the positive relative vorticity and the *line* of the zero-zonal wind at 850 hPa

GRIMs. In the PEA, on the contrary, the simulated track density is closest to the observations in term of pattern and frequency.

These spatial distributions of TC activity can be explained by large-scale circulation patterns. The monsoon trough (i.e., positive relative vorticity) and weak vertical wind shear provide favorable dynamic conditions for TC formation and development over the WNP (Fig. 4). In particular, the monsoon trough is modulated by the low-level circulation pattern such as southwesterly monsoon winds in the tropical WNP (Fig. 5). In the observation, the most TCs are generated in the region where the relative vorticity

is positive or the vertical wind shear is less than 10 m s^{-1} (Figs. 2a, 4a). All RCMs skillfully capture the gross pattern of the observed monsoon trough and vertical wind shear, however, some notable discrepancies should be carefully considered. In HadGEM3-RA, the weakened monsoon trough by the underestimated southwesterly over the SCS and strengthened vertical wind shear along the monsoon trough appear to inhibit TC formation therein (Figs. 2b, 4b, 5b). In RegCM, the monsoon trough is strengthened by the overestimated southwesterly wind over the SCS, and the convergence is strengthened by the distorted wind directions (i.e., northerly biases) over the eastern part of the
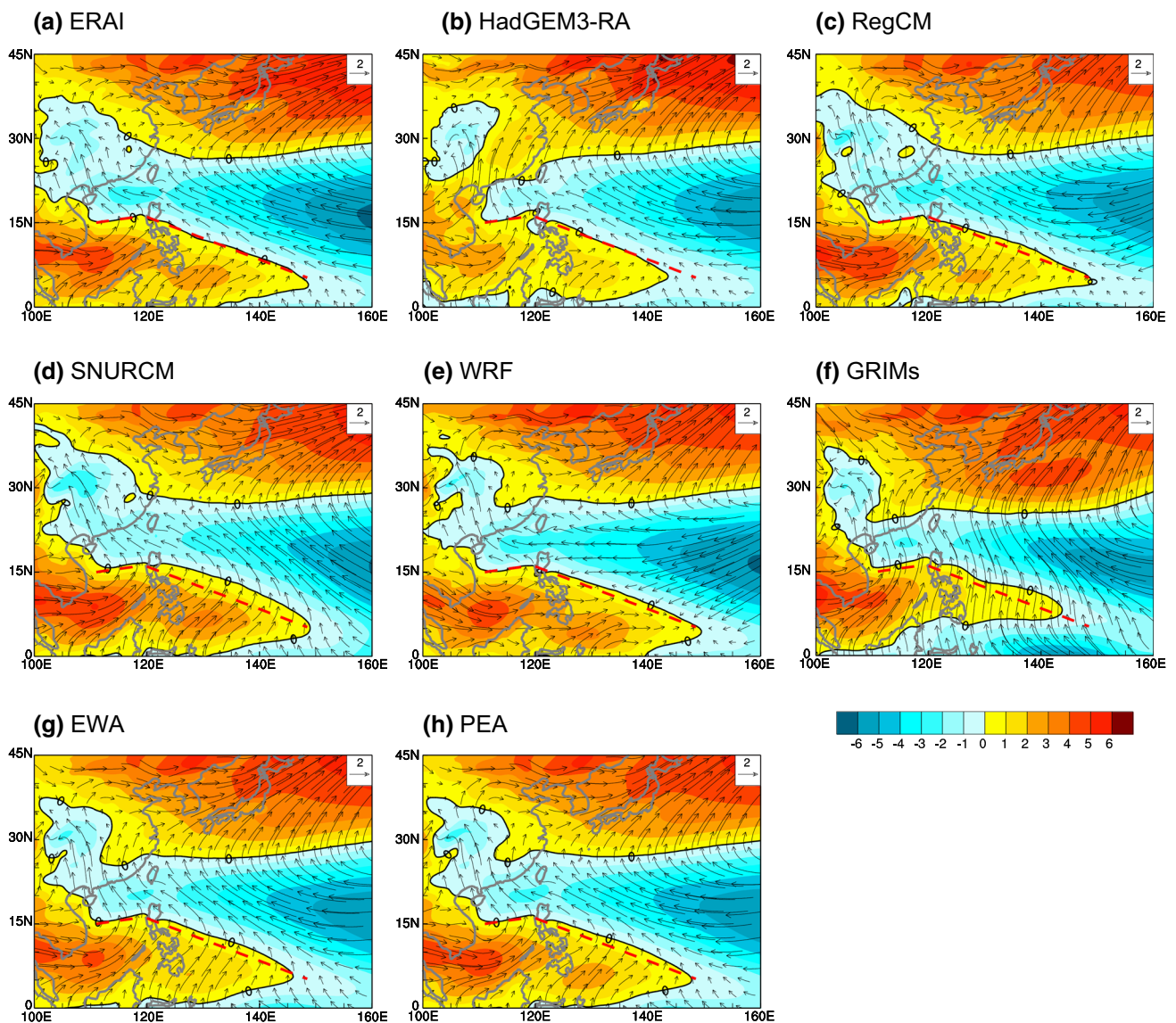
Fig. 5 As in Fig. 4, but for wind (m s^{-1}; *vector*) and zonal wind speed (m s^{-1}; *shading*) at 850 hPa

tropical WNP (Figs. 4c, 5c). These results are associated with the overestimated TC formation over these regions (Fig. 2c). In SNURCM, the monsoon trough seems to expand northward due to the overestimated southwesterly winds over the tropical WNP (Figs. 4d, 5d). These broad difference leads to the overestimated TC activity over the most basin (Figs. 2d, 3d). WRF successfully reproduces the location and strength of the monsoon trough and vertical wind shear, except for the distorted wind directions around the eastern part of the tropical WNP (Figs. 4e, 5e). This discrepancy leads to the slightly overestimated TC formation there but does not prevent it from resulting in the most realistic TC activity among the models (Figs. 2e, 3e). In GRIMs, the monsoon trough (vertical wind shear) is excessively narrower (stronger) due to the overestimated

southerly component of the southwesterly wind over the tropical WNP. Additionally, the upper westerly wind (i.e., high vertical wind shear) in the mid-latitudes is enhanced and expanded southward. Since these circulation patterns provide unfavorable conditions for TC activities, TC formation and tracks are underestimated over the PS and the East Asian coastal area, respectively. In the PEA, the simulated large-scale circulations appear to be closest to those in the observation among the models and EWA.

Through the aforementioned analysis, we found that most of the discrepancies in the large-scale circulation are related to the regional biases in TC activity. The simulated large-scale circulation and TC activity can also be linked to characteristics of each model such as physics scheme and spectral nudging. The cumulus parameterization schemes

used in the three models (Emanuel scheme in RegCM and Kain-Fritsch scheme in SNURCM and WRF) are known to overestimate the convective precipitation and monsoon westerly in the WNP (Cha et al. 2011b, 2015; Chow et al. 2006). However, these potential systematic errors can be reduced by applying the spectral nudging to the models (Feser and von Storch 2008). In turn, these models seem to be able to appropriately reproduce the observed spatial pattern of TC activity through the realistically simulated large-scale circulation by spectral nudging. The full wind (rotational and divergent components) nudging is applied to these models, whereas the only rotational wind nudging is applied to GRIMs (Table 1). For the spectral nudging, the exclusions of observed northerly (southerly) divergent winds at the lower (upper) troposphere lead to southerly (northerly) wind biases there (not shown). These result in the narrow monsoon trough and southward expansion of upper westerly that inhibit TC formation in the PS and TC movement toward the East Asian coastal area. According to

Hong and Chang (2012), the full wind (rotational and divergent components) nudging could alleviate these systematic errors but was not applied to GRIMs used in this study, because it leaded to significantly distorted mass fields aloft. Unlike these models, the spectral nudging is not applied to HadGEM3-RA. This leads to the weakened monsoon trough by the underestimated southwesterly that inhibit TC formation. In addition, the simulated precipitation over the WNP is much smaller than in observations (not shown). Given that simulations without coupled air-sea interaction generally have positive biases in oceanic precipitation (e.g., Cha et al. 2011a; Cha and Lee 2009), the cumulus parameterization scheme resulting in the underestimated oceanic precipitation in HadGEM3-RA may not be appropriate for simulating the convective activity in the tropical WNP. These suggest that the extremely underestimated TC activity in HadGEM3-RA can be associated with not only the dynamically but also the physically unfavorable conditions for TC formation and development.

Fig. 6 Distribution of **a** maximum wind speed and **b** minimum sea level pressure from the RSMC and models for the period 1989–2008
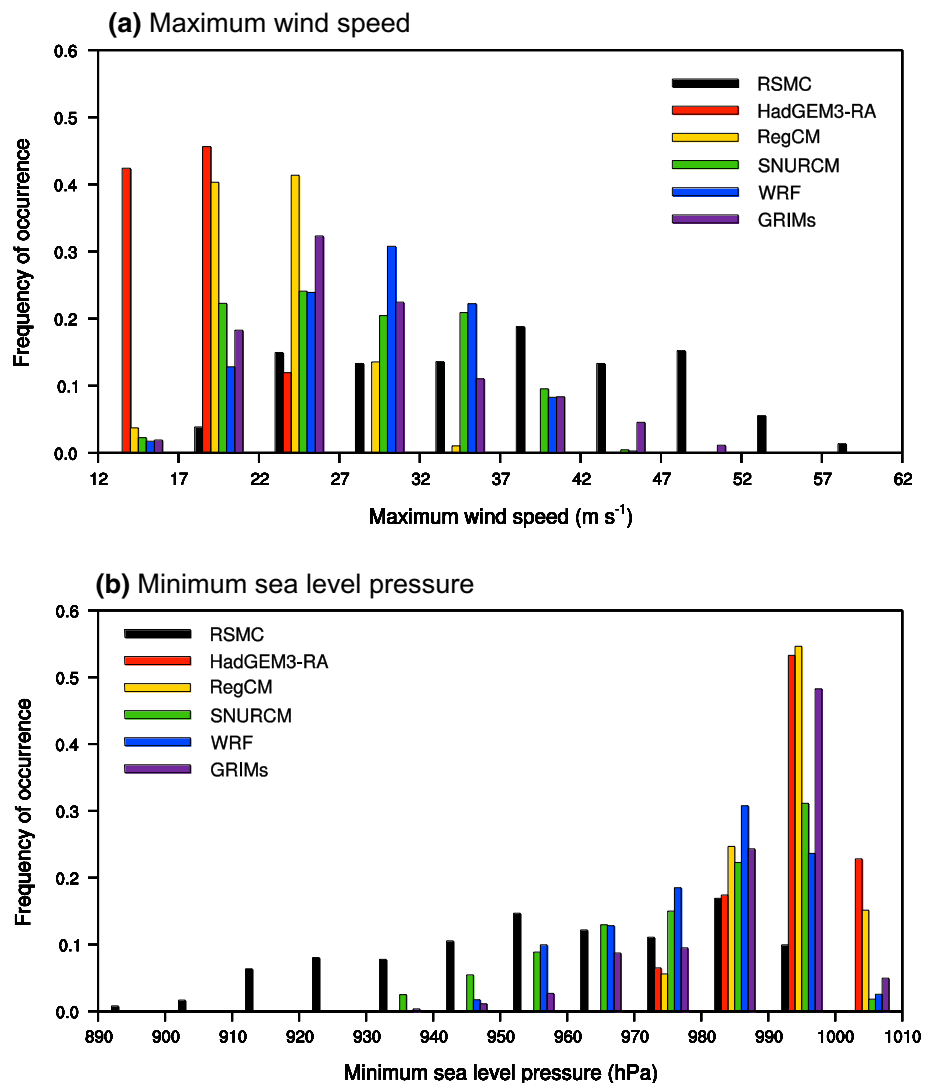
3.2 Intensity distribution

In this section, the distributions of the life-time maximum wind speed and minimum sea level pressure for all RCMs including the wind-pressure relationship are presented. These results can show how the simulated TC intensity varies in models with identical resolution, since the simulated TC intensity depends not only on the horizontal resolution but also on the physics (e.g., Tao et al. 2011).

Figure 6 shows the frequency of occurrence of maximum wind speed and minimum sea level pressure in the observations and models. Since 50-km resolution is not sufficient to resolve intense TCs, both observed variables are uniformly distributed but the simulated ones are skewed toward the weak intensities. In the simulations, there is a qualitative difference between the distributions of maximum wind speed for HadGEM3-RA and RegCM on the one hand, and SNURCM, WRF, and GRIMs on the other. In HadGEM3-RA and RegCM, the distributions are too narrow and skewed toward lower wind speeds, and their right tails above 32 m s^{-1} corresponding to typhoon intensity, are not reproduced at all. In SNURCM, WRF, and GRIMs, the shapes of the distribution become more similar to that in the observations, although these models tend to overestimate (underestimate) wind speeds below (above) 37 m s^{-1}. This discrepancy has been detected in previous studies (Kim et al. 2014a; Murakami and Sugi 2010). It is noteworthy that simulated TCs by HadGEM3-RA do not have higher wind speeds above 27 m s^{-1}, although the model has an advantage in resolving meso-scale convection associated with TC as a non-hydrostatic model. By contrast, GRIMs has a reasonable distribution of winds speeds, similar to the other models, in spite of being a
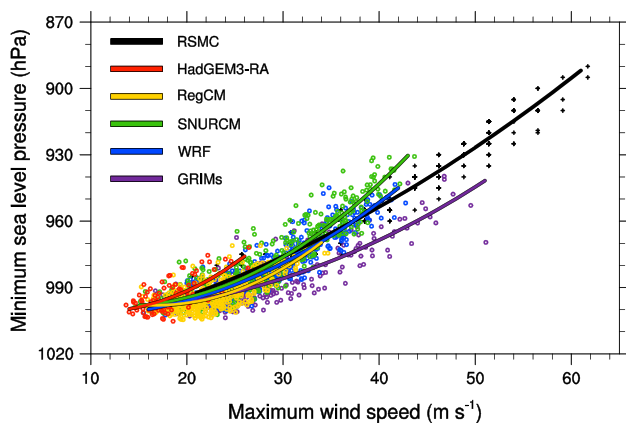
hydrostatic model. Furthermore, GRIMs is the only model that can simulate higher wind speeds sufficiently exceeding 42 m s^{-1}. This is because a revised roughness length formulation based on Donelan et al. (2004) is used to effectively reduce the surface drag coefficient in the presence of high winds. As a result, GRIMs seems to have a reasonable distribution of maximum wind speed. These results suggest that appropriate physics such as surface exchange as well as dynamics such as finer resolution and dynamic framework including finer resolution are important for the simulation of TC intensity.

Except for GRIMs, the distributions of minimum sea level pressure can be explained similarly as that of the aforementioned maximum wind speed. GRIMs seems to overcome the limitation of the hydrostatic model by showing a reasonable distribution of maximum wind speeds, however, there are too many weak TCs with pressures above 990 hPa. In HadGEM3-RA and RegCM, the distributions are too narrow and skewed toward higher sea level pressure, and their left tails below 970 hPa are not reproduced at all. In SNURCM and WRF, although there are still some differences compared to the observation below 970 hPa, the differences become smaller as compared to the other models.

Another way to assess simulated TC intensity is to examine the maximum wind speed with respect to the corresponding sea level pressure. This wind-pressure relationship is shown in Fig. 7, along with the lines denoting the second-order polynomial fit to the data points in the scatter diagram. Regardless of the simulated maximum intensities, HadGEM3-RA and SNURCM have difficulty generating strong enough wind speeds for a given pressure compared to observation. This feature has been attributed to insufficient horizontal resolution (Manganello et al. 2012) and deficiencies in the surface momentum flux parameterization (Powell et al. 2003; Moon et al. 2007). These issues are well known with other current models (e.g., Knutson et al. 2007; Murakami and Sugi 2010). In contrast, the RegCM and GRIMs have difficulty generating stronger wind speeds for a given pressure compared to observations. As the wind speed increases, this deficiency is reduced in RegCM but abnormally increased in GRIMs. This feature of GRIMs is consistent with the distribution that it is reasonable in the wind speed but skewed toward weak intensities in the pressure. This could be because GRIMs has the realistic surface momentum exchange in the high wind speed range but has difficulty in resolving meso-scale convection as a hydrostatic model. WRF is closest to observations compared to the other models.

Fig. 7 Scatter diagram of the lifetime maximum wind speed and minimum sea level pressure in RSMC (*black*), HadGEM3-RA (*red*), RegCM (*yellow*), SNURCM (*green*), WRF (*blue*), and GRIMs (*purple*) for the period 1989–2008. *Solid line* shows the polynomial fit to the data points in the observation and models, respectively

3.3 Interannual variability

The capability of a model to reproduce the observed interannual variability in TC activity is important for assessing

its overall performance in simulating TC activity. Figure 8a represents the time series of the observed and simulated TC genesis frequency. The capability of the models is measured by the RMSE and temporal correlation between observations and simulations (Table 3). HadGEM3-RA and GRIMs have large RMSE (14.0 and 7.9), low values of temporal correlations (not statistically significant 0.38 and 0.07), and a non-decreasing trend. In particular, GRIMs does not capture the observed interannual variation of TC genesis at all. This might be associated with unrealistic large-scale circulation in GRIMs (Fig. 4f). HadGEM3-RA also has relatively low temporal correlation due to the extremely underestimated TC genesis caused by the weakened convective activity over the WNP. This indicates that advancement in the convective parameterization in HadGEM3-RA can lead to an improvement in the interannual variability of the simulated TC genesis.

Overall, RegCM, SNURCM, and WRF skillfully capture well the interannual variations of TC genesis frequency with smaller RMSE (5.1, 6.1, and 4.0), significant temporal correlation (0.56, 0.44, and 0.53), and a decreasing trend, except that SNURCM shows a higher frequency than the observations during the period 1998–2002 which includes El Niño and La Niña event years. SNURCM tends

to overestimate TC genesis in El Niño and La Niña years as compared to neutral years (not shown). RegCM has the highest temporal correlation and WRF has the smallest RMSE as compared to the other models. The temporal correlations in these models are similar or lower than those (0.43–0.75) reported in previous studies (Au-Yeung and Chan 2012; Jin et al. 2013; Zhan et al. 2011; Zhao et al. 2009). Given that the continuous 20-year integration and objectively defined thresholds for TC in this study as compared to the previous studies, which had seasonal integrations and their own preferred thresholds for TC, these models have reasonable capability in capturing the interannual variability of TC genesis. Interestingly, RegCM, SNURCM, and WRF (HadGEM3-RA and GRIMs) show higher (lower) ability in simulating not only the spatial distribution of TC activity but also their interannual variation. This suggests that the models' performances of TC spatial pattern and temporal variation are similar to each other, since the frequency and locations of TC formation are simultaneously modulated by large-scale circulation such as the El Niño-Southern Oscillation (ENSO) and the WNP subtropical high (Ho et al. 2004; Wang and Chan 2002). Similarly, the performances of the interannual variabilities in the two ensemble averages are analogous to those of the spatial distribution. The EWA has a higher temporal correlation coefficient (0.58) than the other models, although HadGEM3-RA and GRIMs have statistically insignificant low correlation coefficients. Furthermore, the PEA generally fares better than the other models; RMSE and temporal correlation are 3.4 and 0.64, respectively.

In addition to TC genesis frequency, we examine the interannual variability of the seasonal accumulated cyclone energy (ACE), which is defined as the sum of the square of the maximum wind speeds during the lifetime of each TC during JJASON (Fig. 8b). The ACE index is useful for understanding the interannual variability of TC activity influenced by the ENSO, because it is positively correlated with the ENSO, which modulates the location of TC formations (Camargo and Sobel 2005). Since TCs in HadGEM3-RA have very weak intensities that seldom exceed the ACE threshold of 17 m s^{-1} (Fig. 6a), we define the ACE in the models, as the sum of the squares of the TC's maximum wind speed, sampled at 6-h intervals without any intensity threshold (e.g., Camargo et al. 2005; Shaevitz et al. 2014). The models, except for HadGEM3-RA (5 %), have roughly 40–70 % of the observed mean ACE (42.9) because of the limitations of the TC-resolving capability in the models with 50-km horizontal resolution. Regardless of these large biases, the temporal correlations coefficients between the observed and simulated ACEs are 0.40–0.79, which is statistically significant at 90–99 %. Besides, these biases tend to be smaller during the La Niña (e.g., 1998 and 1999) years when strong TCs are reduced. In the EWA and PEA, the interannual variability for
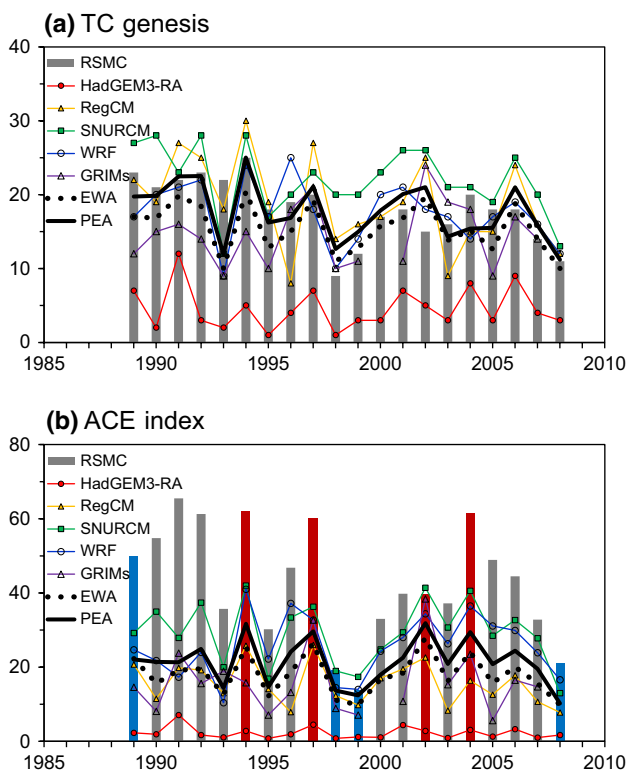

Fig. 8 Annual number of **a** TC genesis and **b** ACE ($10^4 \text{ m}^2 \text{ s}^{-2}$) in RSMC and models during the period 1989–2008. *Red* and *blue bars* show El Niño and La Niña years, respectively

the ACE are comparable to those for TC genesis, although most models largely underestimate the mean ACE.

4 Summary and conclusion

In this study, CORDEX multi-RCMs were evaluated for their ability to capture climatology, intensity and interannual variability of TC activity over the WNP for the period 1989–2008. The multi-RCM ensemble consists of five different RCMs with ~50 km resolution driven by ERA-Interim reanalysis. Performances of the individual models were investigated in detail for TC activity compared to observational datasets.

1. HadGEM3-RA and GRIMs have prominent systematic errors in the spatial patterns of simulated TC activity over the WNP, while RegCM, SNURCM, and WRF tend to simulate them reasonably. In particular, WRF has the most realistic spatial patterns of TC activity compared to the other models and successfully reproduce the observed large-scale environment. On the other hand, HadGEM3-RA largely underestimates TC activity which is associated with unrealistically unfavorable conditions (i.e., weaker monsoon trough and convective activity in the tropical WNP) for TC formation and development.

2. With respect to the distributions of TC intensities, HadGEM3-RA and RegCM appear to have difficulty in reproducing TCs corresponding to typhoon intensity, while SNURCM, WRF, and GRIMs are capable of simulating TCs of this intensity. However, for intense TCs above 47 m s^{-1} and below 930 hPa, all RCMs critically limited, implying that the 50-km resolution is not sufficient to resolve the observed intensity of TCs.

3. HadGEM3-RA and GRIMs do not capture the observed interannual variation of TC genesis frequency with larger RMSE and low correlations, while RegCM, SNURCM, and WRF capture it well with smaller RMSE and high correlations. These two group are identically classified in relation to the spatial pattern of TC activity. Their performances of spatial pattern and interannual variation of simulated TCs correlate with each other, since the frequency and location of TC formation are simultaneously modulated by the large-scale circulation. For the interannual variability of ACE, most models have approximately one half of the observed mean ACE, but they have high correlations.

The individual models have a variety of systematic biases for simulating TCs, however, the ensemble averages successfully capture the spatial and temporal nature of TC activity. In particular, the PEA with smaller biases and

higher correlation generally outperforms individual models and the EWA, since model results are averaged with different weighting based on the model performance. This confirms that the PEA provides the best performance of not only temperature and precipitation mainly applied in previous studies, but also TC activity by reducing the uncertainty in the simulated TC activity by a single RCM. Therefore, we conclude that the multi-RCM ensemble within CORDEX-East Asia can be applied to provide more reliable and credible estimation of future TC activity over the western North Pacific due to climate change.

In the future work, we intend to investigate the change in TC activity in response to two warming scenarios [representative concentration pathway 4.5 (RCP4.5) and RCP8.5] compared to historical simulations using multi-RCMs ensemble evaluated in this study. Furthermore, in order to more reliable climate change projections of TC intensity, the resolution of the CORDEX RCMs should be increased so far as computing resources permit over multi-decadal time scales. At the same time, it is necessary to improve the spectral nudging and physical processes such as convective parameterization and surface momentum flux parameterization.

References

Au-Yeung AYM, Chan JCL (2012) Potential use of a regional climate model in seasonal tropical cyclone activity predictions in the western North Pacific. Clim Dyn 39:783–794

Bender MA, Knutson TR, Tuleya RE, Sirutis JJ, Vecchi GA, Garner ST, Held IM (2010) Modeled impact of anthropogenic warming on the frequency of intense Atlantic hurricanes. Science 327:454–458

Bengtsson L, Bottger H, Kanamitsu M (1982) Simulation of hurricane-type vortices in a general-circulation model. Tellus 34:440–457

Camargo SJ (2013) Global and regional aspects of tropical cyclone activity in the CMIP5 models. J Clim 26:9880–9902

Camargo SJ, Sobel AH (2005) Western North Pacific tropical cyclone intensity and ENSO. J Clim 18:2996–3006

Camargo SJ, Zebiak SE (2002) Improving the detection and tracking of tropical cyclones in atmospheric general circulation models. Weather Forecast 17:1152–1162

Camargo SJ, Barnston AG, Zebiak SE (2005) A statistical assessment of tropical cyclone activity in atmospheric general circulation models. Tellus A 57:589–604

Camargo SJ, Li H, Sun L (2007) Feasibility study for downscaling seasonal tropical cyclone activity using the NCEP regional spectral model. Int J Climatol 27:311–326

Cha DH, Lee DK (2009) Reduction of systematic errors in regional climate simulations of the summer monsoon over East Asia and the western North Pacific by applying the spectral nudging technique. J Geophys Res 114:D14108

Cha DH, Jin CS, Lee DK (2011a) Impact of local sea surface temperature anomaly over the western North Pacific on extreme East Asian summer monsoon. Clim Dyn 37:1691–1705

Cha DH, Jin CS, Lee DK, Kuo YH (2011b) Impact of intermittent spectral nudging on regional climate simulation using Weather Research and Forecasting model. J Geophys Res 116:D10103

Cha DH, Jin CS, Moon JH, Lee DK (2015) Improvement of regional climate simulation of East Asian summer monsoon by coupled air–sea interaction and large-scale nudging. Int J Climatol. doi:10.1002/joc.4349

Chow K, Chan JC, Pal JS, Giorgi F (2006) Convection suppression criteria applied to the MIT cumulus parameterization scheme for simulating the Asian summer monsoon. Geophys Res Lett 33:L24709

Christensen JH, Carter TR, Rummukainen M, Amanatidis G (2007) Evaluating the performance and utility of regional climate models: the PRUDENCE project. Clim Change 81:1–6

Davies T, Cullen MJP, Malcolm AJ, Mawson MH, Staniforth A, White AA, Wood N (2005) A new dynamical core for the Met Office's global and regional modelling of the atmosphere. Quart J R Meteorol Soc 131:1759–1782

Donelan M, Haus B, Reul N, Plant W, Stiassnie M, Graber H, Brown O, Saltzman E (2004) On the limiting aerodynamic roughness of the ocean in very strong winds. Geophys Res Lett 31:L18306

Emanuel KA (1991) A scheme for representing cumulus convection in large-scale models. J Atmos Sci 48:2313–2335

Emanuel K, Sundararajan R, Williams J (2008) Hurricanes and global warming: results from downscaling IPCC AR4 simulations. Bull Am Meteorol Soc 89:347–367

Feser F, von Storch H (2008) A dynamical downscaling case study for typhoons in Southeast Asia using a regional climate model. Mon Weather Rev 136:1806–1815

Fu CB, Wang SY, Xiong Z, Gutowski WJ, Lee DK, McGregor JL, Sato Y, Kato H, Kim JW, Suh MS (2005) Regional climate model intercomparison project for Asia. Bull Amer Meteor Soc 86:257–266

Giorgi F, Jones C, Asrar GR (2009) Addressing climate information needs at the regional level: the CORDEX framework. WMO Bull 58:175–183

Giorgi F, Coppola E, Solmon F, Mariotti L, Sylla MB, Bi X, Elguindi N, Diro GT, Nair V, Giuliani G, Turuncoglu UU, Cozzini S, Guttler I, O'Brien TA, Tawfik AB, Shalaby A, Zakey AS, Steiner AL, Stordal F, Sloan LC, Brankovic C (2012) RegCM4: model description and preliminary tests over multiple CORDEX domains. Clim Res 52:7–29

Gregory D, Rowntree PR (1990) A mass flux convection scheme with representation of cloud ensemble characteristics and stability-dependent closure. Mon Weather Rev 118:1483–1506

Ho CH, Baik JJ, Kim JH, Gong DY, Sui CH (2004) Interdecadal changes in summertime typhoon tracks. J Clim 17:1767–1776

Ho CH, Kim JH, Kim HS, Choi W, Lee MH, Yoo HD, Kim TR, Park S (2013) Technical note on a track-pattern-based model for predicting seasonal tropical cyclone activity over the western North Pacific. Adv Atmos Sci 30:1260–1274

Holtslag AAM, Debruijn EIF, Pan HL (1990) A high-resolution air-mass transformation model for short-range weather forecasting. Mon Weather Rev 118:1561–1575

Hong SY, Chang EC (2012) Spectral nudging sensitivity experiments in a regional climate model. Asia-Pac J Atmos Sci 48:345–355

Hong SY, Pan HL (1998) Convective trigger function for a mass-flux cumulus parameterization scheme. Mon Weather Rev 126:2599–2620

Hong SY, Noh Y, Dudhia J (2006) A new vertical diffusion package with an explicit treatment of entrainment processes. Mon Weather Rev 134:2318–2341

Hong SY, Moon NK, Lim KSS, Kim JW (2010) Future climate change scenarios over Korea using a multi-nested downscaling system: a pilot study. Asia-Pac J Atmos Sci 46:425–435

Hong SY, Park H, Cheong HB, Kim JEE, Koo MS, Jang J, Ham S, Hwang SO, Park BK, Chang EC (2013a) The global/regional integrated model system (GRIMs). Asia-Pac J Atmos Sci 49:219–243

Hong SY, Park H, Cheong HB, Kim JEE, Koo MS, Jang J, Ham S, Hwang SO, Park BK, Chang EC, Li HQ (2013b) The global/regional integrated model system (GRIMs). Asia-Pac J Atmos Sci 49:219–243

Huang WR, Chan JCL (2014) Dynamical downscaling forecasts of Western North Pacific tropical cyclone genesis and landfall. Clim Dyn 42:2227–2237

Huang B, Polanski S, Cubasch U (2015) The assessment of precipitation climatology in an ensemble of CORDEX-East Asia regional climate simulations. Clim Res 64:141–158

Jin CS, Ho CH, Kim JH, Lee DK, Cha DH, Yeh SW (2013) Critical role of northern off-equatorial sea surface temperature forcing associated with Central Pacific El Nino in more frequent tropical cyclone movements toward East Asia. J Clim 26:2534–2545

Kain JS (2004) The Kain-Fritsch convective parameterization: an update. J Appl Meteorol 43:170–181

Kim JH, Ho CH, Chu PS (2010) Dipolar redistribution of summertime tropical cyclone genesis between the Philippine Sea and the northern South China Sea and its possible mechanisms. J Geophys Res-Atmos 115:D06104

Kim D, Jin CS, Ho CH, Kim JH, Kim J (2014a) Climatological features of WRF-simulated tropical cyclones over the western North Pacific. Clim Dyn 44:3223–3235

Kim J, Waliser DE, Mattmann CA, Goodale CE, Hart AF, Zimdars PA, Crichton DJ, Jones C, Nikulin G, Hewitson B, Jack C, Lennard C, Favre A (2014b) Evaluation of the CORDEX-Africa multi-RCM hindcast: systematic model errors. Clim Dyn 42:1189–1202

Knutson TR, Sirutis JJ, Garner ST, Held IM, Tuleya RE (2007) Simulation of the recent multidecadal increase of Atlantic hurricane activity using an 18-km-grid regional model. Bull Am Meteor Soc 88:1549–1565

Landman WA, Seth A, Camargo SJ (2005) The effect of regional climate model domain choice on the simulation of tropical cyclone-like vortices in the southwestern Indian Ocean. J Clim 18:1263–1274

LaRow TE, Lim YK, Shin DW, Chassignet EP, Cocke S (2008) Atlantic basin seasonal hurricane simulations. J Clim 21:3191–3206

Lee JW, Hong SY (2014) Potential for added value to downscaled climate extremes over Korea by increased resolution of a regional climate model. Theor Appl Climatol 117:667–677

Lee DK, Cha DH, Kang HS (2004) Regional climate simulation of the 1998 summer flood over East Asia. J Meteorol Soc Jpn 82:1735–1753

Lee DK, Cha DH, Jin CS, Choi SJ (2013) A regional climate change simulation over East Asia. Asia-Pac J Atmos Sci 49:655–664

Lock AP, Brown AR, Bush MR, Martin GM, Smith RNB (2000) A new boundary layer mixing scheme. Part I: scheme description and single-column model tests. Mon Weather Rev 128:3187–3199

Manganello JV, Hodges KI, Kinter JL, Cash BA, Marx L, Jung T, Achuthavarier D, Adams JM, Altshuler EL, Huang BH, Jin EK, Stan C, Towers P, Wedi N (2012) Tropical cyclone climatology in a 10-km global atmospheric GCM: toward weather-resolving climate modeling. J Clim 25:3867–3893

Moon IJ, Ginis I, Hara T, Thomas B (2007) A physics-based parameterization of air-sea momentum flux at high wind speeds and its impact on hurricane intensity predictions. Mon Weather Rev 135:2869–2878

Murakami H, Sugi M (2010) Effect of model resolution on tropical cyclone climate projections. Sola 6:73–76

Murakami H, Mizuta R, Shindo E (2012a) Future changes in tropical cyclone activity projected by multi-physics and multi-SST ensemble experiments using the 60-km-mesh MRI-AGCM. Clim Dyn 39:2569–2584

Murakami H, Wang Y, Yoshimura H, Mizuta R, Sugi M, Shindo E, Adachi Y, Yukimoto S, Hosaka M, Kusunoki S (2012b) Future changes in tropical cyclone activity projected by the new high-resolution MRI-AGCM. J Clim 25:3237–3260

Oh SG, Suh MS, Cha DH (2013) Impact of lateral boundary conditions on precipitation and temperature extremes over South Korea in the CORDEX regional climate simulation using RegCM4. Asia-Pac J Atmos Sci 49:497–509

Oouchi K, Yoshimura J, Yoshimura H, Mizuta R, Kusunoki S, Noda A (2006) Tropical cyclone climatology in a global-warming climate as simulated in a 20 km-mesh global atmospheric model: frequency and wind intensity analyses. J Meteorol Soc Jpn 84:259–276

Park JH, Oh SG, Suh MS (2013) Impacts of boundary conditions on the precipitation simulation of RegCM4 in the CORDEX East Asia domain. J Geophys Res-Atmos 118:1652–1667

Powell MD, Vickery PJ, Reinhold TA (2003) Reduced drag coefficient for high wind speeds in tropical cyclones. Nature 422:279–283

Shaevitz DA, Camargo SJ, Sobel AH, Jonas JA, Kim D, Kumar A, LaRow TE, Lim YK, Murakami H, Reed KA (2014) Characteristics of tropical cyclones in high-resolution models in the present climate. J Adv Model Earth Syst 6:1154–1172

Skamarock WC, Klemp JB, Dudhia J, Gill DO, Barker DM, Wang W, Powers JG (2008) A description of the advanced research WRF version 3. In: NCAR Tech 15 Note NCAR/TN–475 + STR

Skamarock WC, Klemp JB, Duda MG, Fowler LD, Park SH, Ringler TD (2012) A multiscale nonhydrostatic atmospheric model using centroidal Voronoi tesselations and C-grid staggering. Mon Weather Rev 140:3090–3105

Strachan J, Vidale PL, Hodges K, Roberts M, Demory ME (2013) Investigating global tropical cyclone activity with a hierarchy of AGCMs: the role of model resolution. J Clim 26:133–152

Suh MS, Oh SG, Lee DK, Cha DH, Choi SJ, Jin CS, Hong SY (2012) Development of new ensemble methods based on the performance skills of regional climate models over South Korea. J Clim 25:7067–7082

Tao WK, Shi JJ, Chen SYS, Lang S, Lin PL, Hong SY, Peters-Lidard C, Hou A (2011) The impact of microphysical schemes on hurricane intensity and track. Asia-Pac J Atmos Sci 47:1–16

Vitart F, Anderson JL, Stern WF (1997) Simulation of interannual variability of tropical storm frequency in an ensemble of GCM integrations. J Clim 10:745–760

Walsh KJE, Fiorino M, Landsea CW, McInnes KL (2007) Objectively determined resolution-dependent threshold criteria for the detection of tropical cyclones in climate models and reanalyses. J Clim 20:2307–2314

Walsh KJ, Camargo SJ, Vecchi GA, Daloz AS, Elsner J, Emanuel K, Horn M, Lim Y-K, Roberts M, Patricola C (2015) Hurricanes and climate: the US CLIVAR working group on hurricanes. Bull Am Meteorol Soc 96:997–1017

Wang B, Chan JCL (2002) How strong ENSO events affect tropical storm activity over the Western North Pacific. J Clim 15:1643–1658

Wehner MF, Reed KA, Li F, Bacmeister J, Chen CT, Paciorek C, Gleckler PJ, Sperber KR, Collins WD, Gettelman A (2014) The effect of horizontal resolution on simulation quality in the community atmospheric model, CAM5. 1. J Adv Model Earth Syst 6:980–997

Wu L, Chou C, Chen CT, Huang R, Knutson TR, Sirutis JJ, Garner ST, Kerr C, Lee CJ, Feng YC (2014) Simulations of the present and late-twenty-first-century western North Pacific tropical cyclone activity using a regional model. J Clim 27:3405–3424

Xie PP, Arkin PA (1997) Global precipitation: a 17-year monthly analysis based on gauge observations, satellite estimates, and numerical model outputs. Bull Am Meteorol Soc 78:2539–2558

Zhan RF, Wang YQ, Wu CC (2011) Impact of SSTA in the East Indian Ocean on the frequency of Northwest Pacific tropical cyclones: a regional atmospheric model study. J Clim 24:6227–6242

Zhao M, Held IM (2012) TC-permitting GCM simulations of hurricane frequency response to sea surface temperature anomalies projected for the late-twenty-first century. J Clim 25:2995–3009

Zhao M, Held IM, Lin SJ, Vecchi GA (2009) Simulations of global hurricane climatology, interannual variability, and response to global warming using a 50-km resolution GCM. J Clim 22:6653–6678

Zou LW, Qian Y, Zhou TJ, Yang B (2014) Parameter tuning and calibration of RegCM3 with MIT-Emanuel cumulus parameterization scheme over CORDEX East Asia Domain. J Clim 27:7687–7701